



Steady state effects introduced by local relaxation modes on J-driven DNP-enhanced NMR

Maria Grazia Concilio^{*}, Lucio Frydman

Department of Chemical and Biological Physics, Weizmann Institute of Science, Rehovot, Israel

ARTICLE INFO

Keywords:

Dynamic nuclear polarization
stable biradicals
singlet to triplet cross-relaxation
local mode relaxation

ABSTRACT

One of solution-state Nuclear Magnetic Resonance (NMR)'s main weaknesses, is its relative insensitivity. J-driven Dynamic Nuclear Polarization (JDNP) was recently proposed for enhancing solution-state NMR's sensitivity, by bypassing the limitations faced by conventional Overhauser DNP (ODNP), at the high magnetic fields where most analytical research is performed. By relying on biradicals with inter-electron exchange couplings J_{ex} on the order of the electron Larmor frequency ω_E , JDNP was predicted to introduce a transient enhancement in NMR's nuclear polarization at high magnetic fields, and for a wide range of rotational correlation times of medium-sized molecules in conventional solvents. This communication revisits the JDNP proposal, including additional effects and conditions that were not considered in the original treatment. These include relaxation mechanisms arising from local vibrational modes that often dominate electron relaxation in organic radicals, as well as the possibility of using biradicals with J_{ex} of the order of the nuclear Larmor frequency ω_N as potential polarizing agents. The presence of these new relaxation effects lead to variations in the JDNP polarization mechanism originally proposed, and indicate that triplet-to-singlet cross-relaxation processes may lead to a nuclear polarization enhancement that persists even at steady states. The physics and potential limitations of the ensuing theoretical derivations, are briefly discussed.

1. Introduction

Nuclear Magnetic Resonance (NMR) is one of the most versatile forms of spectroscopy, conveying structural and dynamical information with minimal invasiveness. Even further applications could emerge if it was not for the limited sensitivity of NMR – particularly when executed on room temperature solutions and at high magnetic fields (7 T – 23 T), where most analytical and biophysical studies are performed. The sensitivity of solution state NMR can be enhanced by Overhauser DNP (ODNP) [1–3]; however, when driven by dipolar relaxation mechanisms, ODNP only works efficiently at relatively low magnetic fields [4–7]. High-field ODNP experiments by contrast are usually limited, as they need to be aided by Fermi contact couplings of the kind which arises for certain nuclei such as ^{31}P [8,9], ^{19}F [10,11] and ^{13}C [6,12–14]. Significant scalar-driven DNP enhancements can then arise, but this requires an electron delocalization that only arises in specific radical/solvent combinations. [6,11,15–18]. However, for the more general and highly relevant case, involving ^1H nuclei interacting with electron radicals solely through inter-molecular dipolar hyperfine couplings, ODNP

efficiency decays rapidly with the magnetic field, B_0 . [3,19].

J-driven Dynamic Nuclear Polarization (JDNP) [20] is a recently described theoretical proposal, aiming to enhance NMR's sensitivity in solution state at any magnetic field, solely relying on inter-molecular dipolar hyperfine couplings. As ODNP, JDNP can be conceivably performed either with a microwave irradiation at the electron Larmor frequency or by shuttling the sample between higher and lower magnetic fields, with one of these fields serving to achieve hyperpolarization and the other NMR observation. [21,22] Unlike ODNP, which relies on stable mono-radicals, JDNP relies on stable biradicals with the inter-electron exchange coupling J_{ex} in the range of the electron Larmor frequency ω_E . In such case, Redfield's relaxation theory [23] predicts that at the $J_{ex} \approx \omega_E$ JDNP condition, a difference between the self-relaxation rates of the two-electron singlet and triplet states which are dipolar hyperfine coupled to the α or β nuclear states will arise. This leads to a transient imbalance between the nuclear spin populations, and consequently a transient nuclear polarization build-up.

The current work describes the effects of non-Redfield, field-independent local vibrational modes arising from the mixing between spin

^{*} Corresponding author.

E-mail address: maria-grazia.concilio@weizmann.ac.il (M. Grazia Concilio).

<https://doi.org/10.1016/j.jmr.2023.107542>

Received 22 June 2023; Received in revised form 3 August 2023; Accepted 26 August 2023

Available online 30 August 2023

1090-7807/© 2023 Elsevier Inc. All rights reserved.

and orbital angular momentum, on the JDNP enhancement. Relaxation arising from local vibrational modes driven by spin-orbit coupling, [24–27] often dominate the electron relaxation rates of organic radicals [24,25,27,28]. These effects are shown to lead to steady-state NMR signal enhancements if moderate, and to the suppression of the JDNP phenomena if overtly dominant. For completion this study also considers the possibility of using biradicals with J_{ex} of the order of the nuclear Larmor frequency ω_{N} , for enhancing the sensitivity of solution state NMR at high magnetic fields.

2. Theoretical methodologies

This study's steady state numerical simulations were performed using the Spinach software package [29] based on a laboratory frame Hamiltonian, using the Fokker-Planck formalism described in Ref. [30]. Numerical simulations took account of all self- and cross-relaxation terms within the Bloch-Redfield-Wangsness relaxation theory, [23,31] scalar relaxation of the first kind, [32] and relaxation from a local vibrational mode. Scalar relaxation of the first kind arises from the conformational mobility that modulates the exchange coupling. A “pessimistic” modulation depth of 3 GHz was assumed for this, with a conformational mobility correlation time of 1 picosecond. Still, it was found that these parameters had negligible effects on the JDNP enhancement, since in the $\omega_{\text{E1}} - \omega_{\text{E2}} \rightarrow 0$ scenario here considered – where ω_{E1} and ω_{E2} correspond to the Larmor frequencies of the two electrons – the exchange coupling commutes with the Zeeman interaction leading to no additional relaxation effects.

Relaxation from a local vibrational mode was included as an additional diagonal term in the Redfield relaxation superoperator, applied to the electron longitudinal and transverse states. In the case of trityls, considered here as model systems, local mode relaxation presumably arises due the stretching of the C–S bonds in radical structures and its rate constant is about 6×10^4 Hz; [24–27] this was the value assumed throughout most of our simulations.

The assumed spin system was composed by two electrons and one proton, that interacts solely through dipolar anisotropic hyperfine couplings. Distances between the two unpaired spin-1/2 electrons (belonging to the radical) and the spin-1/2 proton (assumed to belong to a stationary solvent molecule; however, see onwards) were set to 5.5 Å and 13.2 Å respectively (Table 1 reports the actual proton and electron Cartesian coordinates). The electrons' g-tensors were set axially symmetric but non-colinear, with eigenvalues taken from values found in trityls. [33,34] As discussed previously, [22] in the case of axially

Table 1
Biradical / proton spin system parameters used in this paper's simulations.

Parameter	Spin system
¹ H chemical shift tensor, ppm	[555]
Electron 1 g-tensor ¹ eigenvalues, [xx yy zz] / Bohr magneton	[2.0032 2.0032 2.0026]
Electron 1 g-tensor, XYZ active Euler angles / rad	[0.0 0.0 0.0]
Electron 2 g-tensor ¹ eigenvalues, [xx yy zz] / Bohr magneton	[2.0032 2.0032 2.0026]
Electron 2 g-tensor, XYZ active Euler angles / rad	[0.0 $\pi/8$ 0.0]
¹ H coordinates [x y z] / Å	[0.0 5.0 5.0]
Electron 1 and electron 2 coordinates, [x y z] / Å	[0 0–7.20] and [0 7.20]
Rotational correlation time ² τ_{C} / ps	800
Scalar relaxation modulation depth / GHz	3
Scalar relaxation modulation time / ps	1
Local mode relaxation / Hz	6×10^4
Temperature / K	298

¹ Simulations used Zeeman interaction tensors that were made axially symmetric along the main molecular axis (corresponding for instance, to a linker connecting two trityl units).

² Rotational correlation time of the biradical/proton dipolar hyperfine coupled triad.

symmetric g-tensors, rotations perpendicular to the axis along the linker connecting the two monomeric units in a symmetric biradical, could lead to variations that would subtract efficiency from JDNP. These bending angles would be small for short linkers, but could range between $\approx 0^\circ$ and 40° for long linkers containing multiple para-phenylene or acetylene units. [35] Short and long linkers could lead in turn to J_{ex} values ranging from a few 100(s) MHz, to up to 300 GHz [36,37]. For the sake of simplicity, a $\beta = 20^\circ$ bending angle was adopted throughout our calculations; a more comprehensive analysis on the effect of these distortions is presented in Supplementary Information A. All the simulation parameters are summarized in Table 1.

3. Results

3.1. Features of the steady state JDNP

The transient nuclear polarization build-up obtained in the previously mentioned JDNP study, based only on the Redfield relaxation superoperator model, [20] becomes stable at a non-zero steady state when relaxation from local vibrational modes are included in the relaxation superoperator. [29,31] Fig. 1 shows this effect, with an increase of the DNP enhancement with an increase of the microwave nutation power. As can be seen, when the microwave nutation rates become comparable or higher than the magnitude of the relaxation rate arising from the local vibrational mode (which in the present model dominates the electron relaxation rate), a significant steady state enhancement of the nuclear polarization can be achieved. At 9.4 T, where microwave nutation powers of up to about 4 MHz have been reported, [38] high enhancements will arise even if local mode relaxation rates are allowed to increase to 1 MHz – a typical value observed for organic monoradicals in fluid solutions. [26,27,39].

Fig. 2 shows how the nuclear magnetization enhancement depends on the isotropic exchange coupling between the electrons, as a function of magnetic field B_0 . A continuous on-resonance microwave irradiation at the electron Larmor frequency of the biradicals was assumed, and steady state nuclear polarizations were calculated. A significant steady state enhancement is predicted at the $J_{\text{ex}} = \omega_{\text{E}} + \omega_{\text{N}}$ condition; a more modest but still sizable enhancement is also expected at the condition $J_{\text{ex}} = \omega_{\text{N}}$. Notice that the JDNP enhancement's “width” is $(\omega_{\text{E}} + \omega_{\text{N}}) \pm 2$ GHz at any field for the $J_{\text{ex}} = \omega_{\text{E}} + \omega_{\text{N}}$ condition, while it depends on the magnetic field for the $J_{\text{ex}} = \omega_{\text{N}}$ case. For example at 9.4 T, the JDNP enhancement is achieved within ca. $\omega_{\text{N}} \pm 200$ MHz.

Fig. 3 shows the performance predicted for steady-state JDNP effects as compared with the conventional Overhauser DNP, at different magnetic fields, microwave nutation powers and rotational correlation times, τ_{C} . As expected, the ODNP enhancement, based solely on dipolar hyperfine couplings, is strong when the magnetic field is about 0.5 T, but it decays to negligible values at magnetic fields ≥ 1 T, when the rotational correlation time is ≥ 150 ps. The JDNP enhancement, by contrast, remains strong at any magnetic field, and increases with the τ_{C} , at both the $J_{\text{ex}} = \omega_{\text{E}} + \omega_{\text{N}}$ and $J_{\text{ex}} = \omega_{\text{N}}$ conditions. In the case of $J_{\text{ex}} = \omega_{\text{E}} + \omega_{\text{N}}$, the DNP enhancement increases with the microwave nutation power, while for this set of simulation parameters it decreases with the power in the case of $J_{\text{ex}} = \omega_{\text{N}}$, after having reached a maximum at about 200 kHz at 5 T.

3.2. The physics of the steady state JDNP

The electron relaxation and the spin dynamics were examined in this study using the singlet and triplet basis sets. This is justified by the $J_{\text{ex}} \gg \omega_{\text{E1}} - \omega_{\text{E2}}$ scenario, where the electron Zeeman eigenstates are no longer eigenfunctions of the spin Hamiltonian; it is therefore convenient to treat the Hamiltonian in the singlet/triplet electron basis set. Further, as the two electrons are considered localized in different radical monomers, the zero-field splitting is expected to be negligible with respect to the Zeeman interaction, and it was not here included in the

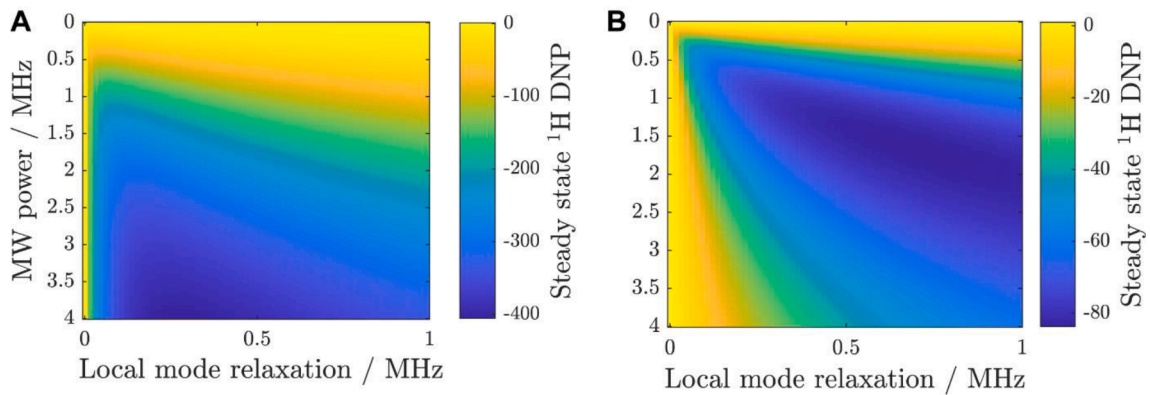


Fig. 1. Simulated DNP enhancements expected at 9.4 T upon continuous microwave irradiation as a function of the microwave power (γB_1 nutation frequencies) and of the magnitude local mode relaxation rate, applied to the diagonal terms in the Redfield relaxation superoperator. Conditions explored $J_{\text{ex}} = \omega_E + \omega_N$ in (A) and $J_{\text{ex}} = \omega_N$ in (B). In this and other figures shown below, the DNP enhancements denote the achieved nuclear polarization, normalized by its Boltzmann counterpart at the same temperature and field. The simulation parameters are given in Table 1.

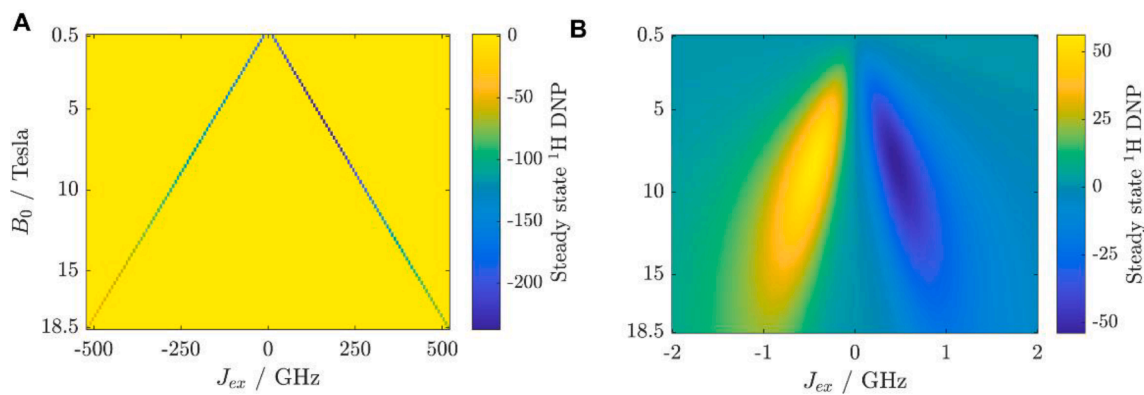


Fig. 2. Simulated DNP enhancements arising at the steady state, assuming a continuous microwave irradiation of a biradical with a nutation frequency of 500 kHz, as a function of J_{ex} and of B_0 . The J_{ex} was changed in between -500 and $+500$ GHz range in (A) and between -2000 and $+2000$ MHz range in (B). Additional simulation parameters are given in Table 1.

Hamiltonians. [40] By contrast, inter – electron dipolar interactions were included in both the spin Hamiltonian and relaxation superoperator in all the simulations; notice that the modulation of these inter-electron dipolar interactions does not contribute to the JDNP mechanism, but only to the electron T_1 and T_2 . [20].

The physics of the JDNP can then be described using three-spin population operators, corresponding to the α and β nuclear components of the two-electron singlet and triplet states (\hat{T}_+ , \hat{T}_0 , \hat{T}_- and \hat{S}_0). [41,42] An alternative description of JDNP's physics can be done using Cartesian operators, by examining the cross-relaxation rate $\hat{E}_Z \rightarrow \hat{N}_Z$; this is analogous to what is usually done in ODNP, and is discussed in the Supporting Material. The steady state effect introduced in Figs. 1-3 can be explained considering the Liouvillian:

$$\hat{L} = \hat{H} + i\hat{R} \quad (1)$$

where \hat{R} is the Redfield relaxation superoperator and \hat{H} is the spin Hamiltonian for a three-spin system composed by two electrons and one proton:

$$\hat{H} = (\omega_E + \omega_{\text{off}})(\hat{E}_{1Z} + \hat{E}_{2Z}) - \omega_N \hat{N}_Z + J_{\text{ex}}(\hat{E}_{1X}\hat{E}_{2X} + \hat{E}_{1Y}\hat{E}_{2Y} + \hat{E}_{1Z}\hat{E}_{2Z}) + \omega_{\text{MW}}(\hat{E}_{1X} + \hat{E}_{2X}) \quad (2)$$

where $\omega_{\text{off}} = \omega_E - \omega_e$ is the offset between the radical Larmor frequency and the free electron frequency; ω_{MW} is the micro-wave irradiation power. Terms describing the secular and pseudo-secular dipolar hyper-

fine interactions (in the order of MHz) are here neglected when compared to terms describing Zeeman and inter-electron exchange interactions (in the order of GHz) – even if they were accounted for and take part in the JDNP mechanism via the relaxation superoperator (as explained below). Although for simplicity these terms are omitted from the spin Hamiltonian in Eq. (2), the full spin Hamiltonian and its singlet/triplet representation is shown in the supporting material of [20]. The spin Hamiltonian in Eq. (2) corresponds to a matrix that can be diagonalized, yielding eigenvalues and eigenstates. For the nuclear α states these eigenvalues correspond to:

$$E_1 = -\frac{3J_{\text{ex}}}{4} + \frac{\omega_N}{2} \rightarrow |\hat{S}_{0,\alpha}\rangle, \quad E_2 = \frac{J_{\text{ex}}}{4} + \frac{\omega_N}{2} + \sqrt{\omega_{\text{MW}}^2 + (\omega_{\text{off}} + \omega_E)^2} \rightarrow |\hat{T}_{+,\alpha}\rangle, \\ E_3 = \frac{J_{\text{ex}}}{4} + \frac{\omega_N}{2} \rightarrow |\hat{T}_{0,\alpha}\rangle, \quad E_4 = \frac{J_{\text{ex}}}{4} + \frac{\omega_N}{2} - \sqrt{\omega_{\text{MW}}^2 + (\omega_{\text{off}} + \omega_E)^2} \rightarrow |\hat{T}_{-,\alpha}\rangle, \quad (3)$$

While for the β states they correspond to:

$$E_5 = -\frac{3J_{\text{ex}}}{4} - \frac{\omega_N}{2} \rightarrow |\hat{S}_{0,\beta}\rangle, \quad E_6 = \frac{J_{\text{ex}}}{4} - \frac{\omega_N}{2} + \sqrt{\omega_{\text{MW}}^2 + (\omega_{\text{off}} + \omega_E)^2} \rightarrow |\hat{T}_{+,\beta}\rangle, \\ E_7 = \frac{J_{\text{ex}}}{4} - \frac{\omega_N}{2} \rightarrow |\hat{T}_{0,\beta}\rangle, \quad E_8 = \frac{J_{\text{ex}}}{4} - \frac{\omega_N}{2} - \sqrt{\omega_{\text{MW}}^2 + (\omega_{\text{off}} + \omega_E)^2} \rightarrow |\hat{T}_{-,\beta}\rangle, \quad (4)$$

At $t = 0$, when $\omega_{\text{MW}} = 0$, the eigenvalues of the α states become equal to:

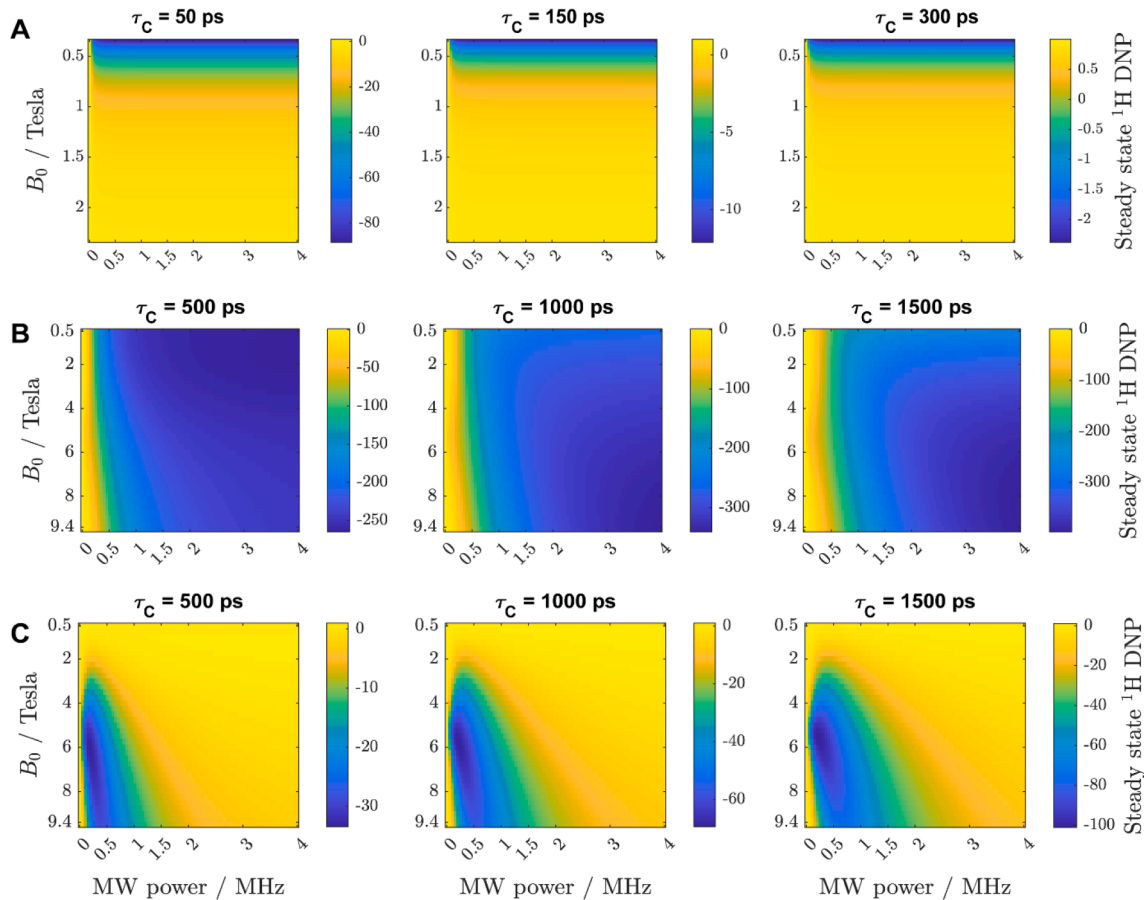


Fig. 3. Simulated DNP enhancements expected upon continuous on-resonance microwave irradiation at the electron Larmor frequency of the biradical, as a function of the magnetic field, of the microwave nutation power, and of the correlation time τ_c in (A) ODNP, (B) JDNP with $J_{ex} = \omega_E + \omega_N$ and (C) JDNP with $J_{ex} = \omega_N$. Notice that each plot has its own colorbar scale. The simulation parameters are given in the Table 1.

$$E_1(0) = -\frac{3J_{ex}}{4} + \frac{\omega_N}{2} \rightarrow |\hat{S}_{0,\alpha}\rangle, \quad E_2(0) = \frac{J_{ex}}{4} + \frac{\omega_N}{2} + \omega_{off} + \omega_E \rightarrow |\hat{T}_{+, \alpha}\rangle, \quad (5)$$

$$E_3(0) = \frac{J_{ex}}{4} + \frac{\omega_N}{2} \rightarrow |\hat{T}_{0,\alpha}\rangle, \quad E_4(0) = \frac{J_{ex}}{4} + \frac{\omega_N}{2} + \omega_{off} - \omega_E \rightarrow |\hat{T}_{-, \alpha}\rangle,$$

and the eigenvalues of the β states become equal to:

$$E_5(0) = -\frac{3J_{ex}}{4} - \frac{\omega_N}{2} \rightarrow |\hat{S}_{0,\beta}\rangle, \quad E_6(0) = \frac{J_{ex}}{4} - \frac{\omega_N}{2} + \omega_{off} + \omega_E \rightarrow |\hat{T}_{+, \beta}\rangle, \quad (6)$$

$$E_7(0) = \frac{J_{ex}}{4} - \frac{\omega_N}{2} \rightarrow |\hat{T}_{0,\beta}\rangle, \quad E_8(0) = \frac{J_{ex}}{4} - \frac{\omega_N}{2} + \omega_{off} - \omega_E \rightarrow |\hat{T}_{-, \beta}\rangle,$$

The energy of the eigenstates in Eqs. (5) and (6) can be arranged from low to high; in the case of negative $J_{ex} \approx \omega_E$, the order is:

$$E_4 < E_8 < E_3 < E_7 < E_1 < E_2 < E_5 < E_6 \quad (7)$$

with $E_1 \sim E_2 \sim E_5 \sim E_6$. In the case of positive $J_{ex} \approx \omega_N$, the order is:

$$E_4 < E_8 < E_1 < E_3 < E_5 < E_7 < E_2 < E_6 \quad (8)$$

with $E_1 \sim E_3 \sim E_5 \sim E_7$. In the absence of microwave irradiation, this leads to the thermal equilibrium populations shown in the central panels of Fig. 4A and 4B (MW power = 0).

When on-resonance microwave irradiation is applied at the electron Larmor frequency of the radical, meaning $-\omega_{off} = \omega_E$, the eigenvalues in Eq. (5) become:

$$E_1(t) = -\frac{3J_{ex}}{4} + \frac{\omega_N}{2} \rightarrow |\hat{S}_{0,\alpha}\rangle, \quad E_2(t) = \frac{J_{ex}}{4} + \frac{\omega_N}{2} + \omega_{MW} \rightarrow |\hat{T}_{+, \alpha}\rangle, \quad (9)$$

$$E_3(t) = \frac{J_{ex}}{4} + \frac{\omega_N}{2} \rightarrow |\hat{T}_{0,\alpha}\rangle, \quad E_4(t) = \frac{J_{ex}}{4} + \frac{\omega_N}{2} - \omega_{MW} \rightarrow |\hat{T}_{-, \alpha}\rangle,$$

corresponding to the indicated eigenstates, while the eigenvalues in Eq. (6) become:

$$E_5(t) = -\frac{3J_{ex}}{4} - \frac{\omega_N}{2} \rightarrow |\hat{S}_{0,\beta}\rangle, \quad E_6(t) = \frac{J_{ex}}{4} - \frac{\omega_N}{2} + \omega_{MW} \rightarrow |\hat{T}_{+, \beta}\rangle, \quad (10)$$

$$E_7(t) = \frac{J_{ex}}{4} - \frac{\omega_N}{2} \rightarrow |\hat{T}_{0,\beta}\rangle, \quad E_8(t) = \frac{J_{ex}}{4} - \frac{\omega_N}{2} - \omega_{MW} \rightarrow |\hat{T}_{-, \beta}\rangle,$$

where the associated states are also indicated. The microwaves do not affect the populations of the $\hat{S}_{0,\alpha/\beta}$ and $\hat{T}_{0,\alpha/\beta}$ states, but they will lead to the decrease/increase in the energy of the $\hat{T}_{+, \alpha/\beta}$ and $\hat{T}_{-, \alpha/\beta}$ states, that will then approach the energy of the $\hat{T}_{0,\alpha/\beta}$ states (Fig. 4). The left panels in Fig. 4, show the electronic saturation as a function of the microwave power. In the presence of microwave irradiation the triplet states are brought out of the thermal equilibrium, and a population imbalance between \hat{T}_+ and \hat{T}_- is transferred to a population imbalance between \hat{T}_0 and \hat{S}_0 (see Fig. 4, left panels). In the case of $J_{ex} \approx \omega_E$, the maximum enhancement is achieved when the electron is fully saturated (meaning $\hat{E}_Z = \hat{T}_+ - \hat{T}_- = 0$, which in this case occurs with $\omega_{MW} > 4$ MHz); a maximum imbalance between the α and β nuclear components of the triplet states is then obtained, as shown in the central panel of Fig. 4A. In the case of $J_{ex} \approx \omega_N$, the maximum enhancement is achieved when the maximum imbalance between the \hat{T}_0 and \hat{S}_0 states is obtained. This does not happen when the electron is fully saturated, but rather when maximal differences between the α and β nuclear components of the triplet states is present (Fig. 4B, central panel). This explains the difference between the monotonic increase of the JDNP enhancement with microwave power arising in the $J_{ex} = \omega_E + \omega_N$ case, vs the

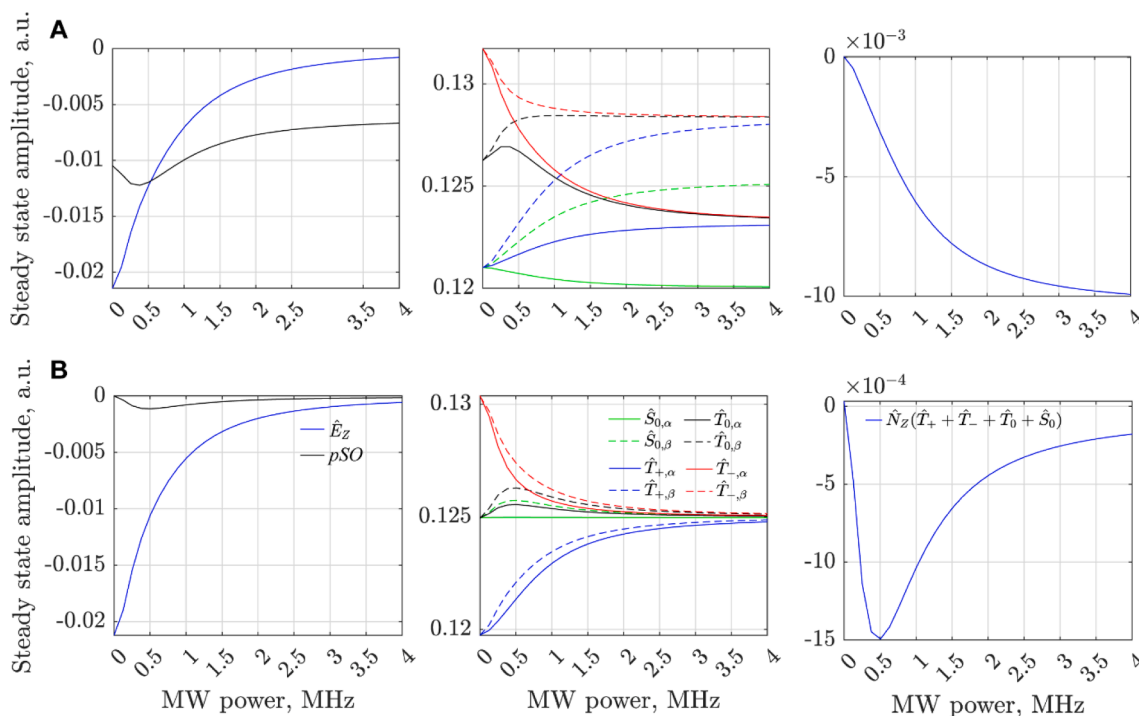


Fig. 4. Dependence of the steady states achieved by various spin states on the microwave nutation power, for a spin system fulfilling $J_{\text{ex}} = \omega_{\text{E}} + \omega_{\text{N}}$ (A), or $J_{\text{ex}} = \omega_{\text{N}}$ (B). *Left-hand panels:* difference between the \hat{T}_+ and \hat{T}_- states, corresponding to the electron longitudinal magnetization, \hat{E}_Z , and between the \hat{T}_0 and \hat{S}_0 states, corresponding to the pseudo singlet order $pSO = -\hat{E}_{1-}\hat{E}_{2+} - \hat{E}_{1+}\hat{E}_{2-}$. *Center panels:* amplitude of the α and β nuclear components of the singlet and triplet states. *Right-hand panels:* longitudinal nuclear magnetization \hat{N}_Z , arising from the sum of the $\hat{N}_Z\hat{T}_+$, $\hat{N}_Z\hat{T}_0$, $\hat{N}_Z\hat{T}_-$ and $\hat{N}_Z\hat{S}_0$ components, according to Eq. (15). All simulations were performed assuming 9.4 T using the parameters given in Table 1.

maximum enhancement observed at about 0.5 MHz that decreases with further microwave power in the case of $J_{\text{ex}} = \omega_{\text{N}}$ (e.g., Fig. 3).

In the presence of relaxation due to local vibrational modes, the self-relaxation rates of the α and β nuclear components of the singlet and of the triplet states become of comparable magnitude (see Figures S2 and S3 in the Supporting Material). Therefore, within the framework described so far, the imbalance between their populations is suppressed, and with it the nuclear polarization enhancement. The creation of a steady state DNP enhancement is thus created by a different mechanism in the presence of the local vibrational relaxation. This DNP enhancement, which was exemplified in Figs. 1-3, can be explained using cross-relaxation arguments akin to those arising in ODNP. Specifically:

1) JDNP mechanism for a biradical with $J_{\text{ex}} \approx \omega_{\text{E}}$

Fig. 5 shows the difference between the cross-relaxation rates among the $\hat{T}_{+\beta}$ and $\hat{S}_{0\alpha}$ and among the $\hat{T}_{+\alpha}$ and $\hat{S}_{0\beta}$ states, as a function of magnetic field and of J_{ex} in the presence of both Redfield and non-Redfield (local) relaxation terms. Notice the marked differences that arise in these rates when the condition $J_{\text{ex}} \approx \omega_{\text{E}}$ is fulfilled (assuming here a negative inter-electron exchange coupling; otherwise the condition $J_{\text{ex}} \approx -\omega_{\text{E}}$ would have to be fulfilled). This difference arises due to the presence of different denominators in the cross-relaxation rates, that becomes relevant when the condition $J_{\text{ex}} \approx \omega_{\text{E}}$ is satisfied:

$$\sigma_{\hat{T}_{+\beta}, \hat{S}_{0\alpha}} = -\frac{\Delta_{\text{HFC}}^2}{180} J(J_{\text{ex}} - \omega_{\text{E}} + \omega_{\text{N}}) \quad (11)$$

$$\sigma_{\hat{T}_{+\alpha}, \hat{S}_{0\beta}} = -\frac{\Delta_{\text{HFC}}^2}{30} J(J_{\text{ex}} - \omega_{\text{E}} - \omega_{\text{N}}) \quad (12)$$

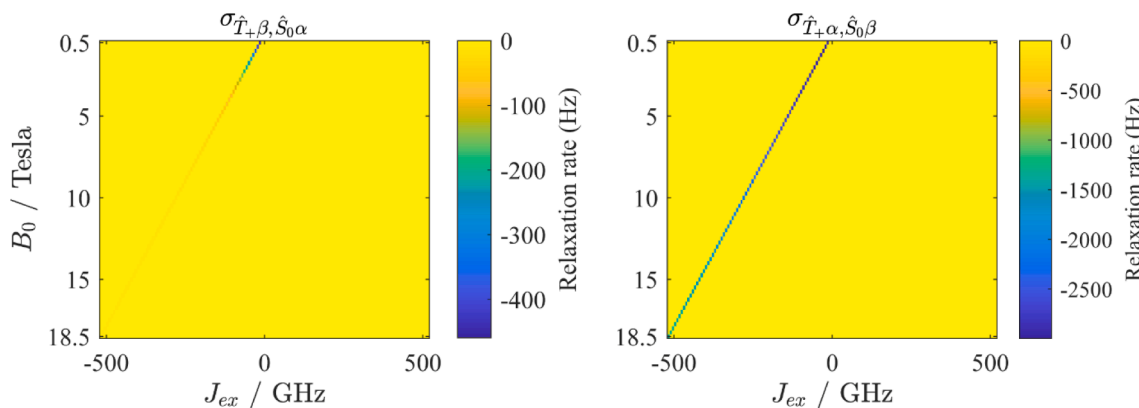


Fig. 5. Triplet to singlet cross-relaxation rates $\sigma_{\hat{T}_{+\beta}, \hat{S}_{0\alpha}}$ and $\sigma_{\hat{T}_{+\alpha}, \hat{S}_{0\beta}}$ as a function of the J_{ex} ranging between -500 GHz and $+500$ GHz and of the magnetic field. Simulation parameters are given in the Table 1.

Here the Δ_{HF}^2 term is the second rank norm squared [20,43] arising from anisotropies associated to the difference between the hyperfine coupling tensors arising due to the interaction between the proton and the two electrons in the system; and $J(\omega)$ is the spectral density function at a frequency ω , corresponding to $\tau_c/(1 + \tau_c^2\omega^2)$. A similar discussion can be made also in the case of a positive $J_{\text{ex}} \approx -\omega_E$, leading to $\sigma_{\hat{T}_{-\beta}, \hat{S}_{0\alpha}} > \sigma_{\hat{T}_{-\alpha}, \hat{S}_{0\beta}}$ at any magnetic field.

2) JDNP mechanism for a biradical with $J_{\text{ex}} \approx \omega_N$

Fig. 6 shows the difference between the cross-relaxation rates among $\hat{S}_{0,\alpha}$ and $\hat{T}_{0,\beta}$ states and among the $\hat{S}_{0,\beta}$ and $\hat{T}_{0,\alpha}$ states with the magnetic field and with J_{ex} , that occurs when the condition $J_{\text{ex}} \approx \omega_N$ is fulfilled. The difference between the triplet to singlet cross-relaxation rates arises this time due to the presence of $(J_{\text{ex}} - \omega_N)$ and $(J_{\text{ex}} + \omega_N)$ in the denominators of the spectral density functions describing the rates:

$$\sigma_{\hat{T}_{0\beta}, \hat{S}_{0\alpha}} = -\frac{\Delta_{\text{HFC}}^2}{60} J(J_{\text{ex}} - \omega_N) \quad (13)$$

$$\sigma_{\hat{T}_{0\alpha}, \hat{S}_{0\beta}} = -\frac{\Delta_{\text{HFC}}^2}{60} J(J_{\text{ex}} + \omega_N) \quad (14)$$

This difference is maximized when the condition $J_{\text{ex}} = \omega_N$ is fulfilled.

4. Discussion and conclusions

The present study revisited the proposal for enhancing NMR signals in solution state at any magnetic field and for a wide range of rotational correlation times, solely relying on inter-molecular dipolar hyperfine couplings and the presence of polarizing biradicals with either $J_{\text{ex}} \approx \omega_E$ or $J_{\text{ex}} \approx \omega_N$. In the previous study, which neglected relaxation from local vibrational modes, the JDNP condition led to a transient imbalance between the α and β nuclear components of singlet and triplet state populations, and consequently to a transient nuclear magnetization build-up. The addition of relaxation from local vibrational modes to the Redfield relaxation superoperator, suppresses the transient nature of this imbalance and leads to a steady state enhancement, akin to that arising in ODNP. However, unlike steady state ODNP effects whose enabling cross-relaxation rates decay quadratically with the strength of the magnetic field, the JDNP effects are only weakly dependent on magnetic fields. Thus, if the available microwave nutation powers are sufficiently high to compete with the triplets' self-relaxation rates ($\approx 10^5$ Hz), a cross-relaxation process between the out-of-the-equilibrium triplet states – either the \hat{T}_{\pm} in the $J_{\text{ex}} \approx \omega_E$ case or the \hat{T}_0 in the $J_{\text{ex}} \approx \omega_N$ case – and the singlet state, will take place. When either the conditions $J_{\text{ex}} \approx \pm\omega_E$ or $J_{\text{ex}} \approx \pm\omega_N$ are fulfilled, these triplet-to-singlet cross-relaxation rates will occur with different rates for α and β states (Eqs. (11) –

(12) and Eqs. (13) – (14). This leads to an imbalance between the populations of α and β nuclear components, and consequently to the creation of longitudinal nuclear polarization in according to:

$$\begin{aligned} \hat{N}_Z &= (\hat{T}_{+\alpha} - \hat{T}_{+\beta}) + (\hat{T}_{0,\alpha} - \hat{T}_{0,\beta}) + (\hat{T}_{-\alpha} - \hat{T}_{-\beta}) + (\hat{S}_{0,\alpha} - \hat{S}_{0,\beta}) \\ &= \hat{N}_Z \hat{T}_+ + \hat{N}_Z \hat{T}_0 + \hat{N}_Z \hat{T}_- + \hat{N}_Z \hat{S}_0 \end{aligned} \quad (15)$$

These differences are the ones shown on the right-hand side of Fig. 4, evidencing the enhancement of the nuclear polarization. Notice that due to the cancellation of the electron or the nuclear Larmor frequencies in the dominators of the spectral density functions arising under JDNP, these cross-relaxation rates are solely dependent on dipolar hyperfine interactions; hence the weak field dependencies shown in Fig. 2. Notice as well that while in the $J_{\text{ex}} \approx \omega_E$ case the sign of the enhancement is always negative, for $J_{\text{ex}} \approx \omega_N$ the sign of the enhancement will change together with the sign of the J_{ex} (see Supporting Material for more details).

The present study assumed a fixed electrons-nuclear geometry. In realistic cases, the nuclear polarization build-up will be interrupted by diffusion of the proton being enhanced, out of the polarization region where JDNP is active and into non-enhancing regions. Under continuous microwave irradiation, however, a steady state enhancement is still expected to arise, as the proton diffuses from one polarizing environment into another in the solution; this is further discussed in the Supporting material.

Another issue further discussed in the Supporting material is the slight increase in the JDNP enhancement with rotational correlation time shown in Fig. 3. This reflects the increased differences between the α/β and the β/α cross-relaxation rates with magnetic field, as expected from the spectral density changes at the JDNP conditions. Notice, however, that in actual cases singlet and triplet self-relaxation rates will also depend on the g -anisotropy, [20,22] and that a large difference between these would lead to a decrease of the triplet T_1 (s), subtracting efficiency from JDNP. Therefore, the ideal biradicals for these JDNP experiments would be those connecting two identical monomers, with axially symmetric g -tensors; these are often found in bistrityls, [33] with a linear, short, conformationally rigid linker. Inter-electron exchange couplings in the order of the electron Larmor frequency can be achieved by linking these radicals with a single para-phenylene unit, leading to a J_{ex} of $\approx 240 \pm 25$ GHz [36]. Inter-electron exchange couplings in the order of the nuclear Larmor frequency can be achieved by lengthening the linker. [37] By contrast, nitroxide biradicals are not suitable for JDNP due to their large g -tensor anisotropy that increases with the magnetic field, contributing to shortening the electron's T_1 and subtracting efficiency to the JDNP process. Pure hydrocarbon-based biradicals, characterized by axial g -tensors with less anisotropy and characterized by slower electron relaxation rates [39], are expected to

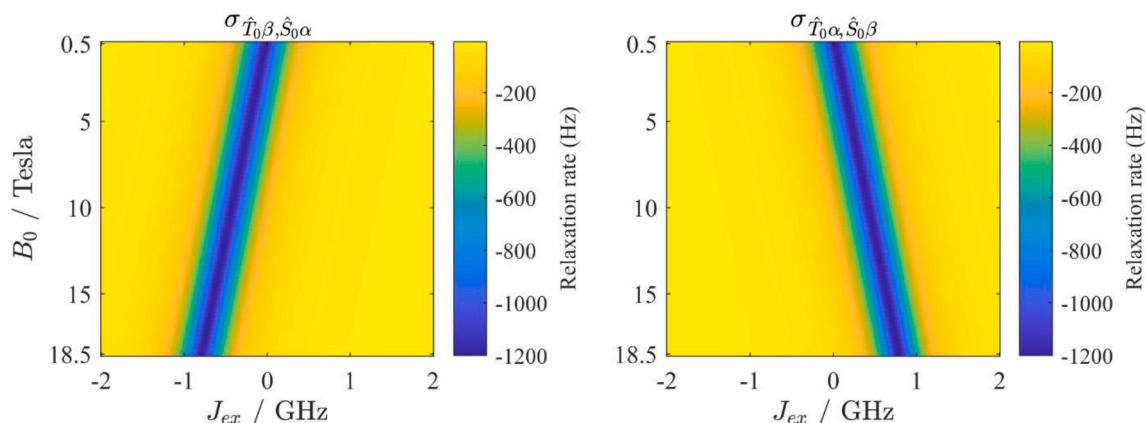


Fig. 6. Triplet to singlet cross-relaxation rates $\sigma_{\hat{T}_{0\beta}, \hat{S}_{0\alpha}}$ and $\sigma_{\hat{T}_{0\alpha}, \hat{S}_{0\beta}}$ as a function of the J_{ex} and of the magnetic field. The simulation parameters are given in the Table 1.

be the most promising polarizing agents for JDNP. Electron Paramagnetic Resonance (EPR) / DNP instrumentation operating at high magnetic field [12,38,44] and equipped with suitable microwave power sources, [38] could enable the observation of the JDNP and development of the optimal polarizing agents.

Declaration of Competing Interest

The authors declare that they have no known competing financial interests or personal relationships that could have appeared to influence the work reported in this paper.

Data availability

Data will be made available on request.

Acknowledgments

This project was funded by the Israel Science Foundation (ISF 1874/22), the Minerva Foundation (Germany), and the USA National Science Foundation (grants number CHE-2203405). MGC acknowledges Weizmann's Faculty of Chemistry for a Dean Fellowship. LF holds the Bertha and Isadore Gudelsky Professorial Chair and Heads the Clore Institute for High-Field Magnetic Resonance Imaging and Spectroscopy whose support is acknowledged, as is the generosity of the Perlman Family Foundation. The authors acknowledge Prof. Ilya Kuprov, Prof. Olav Schiemann and Mr Kevin Kopp for discussions.

Appendix A. Supplementary material

Supplementary data to this article can be found online at <https://doi.org/10.1016/j.jmr.2023.107542>.

References

- [1] A.W. Overhauser, Polarization of nuclei in metals, *Phys. Rev.* 92 (1953) 411.
- [2] T.R. Carver, C.P. Slichter, Experimental verification of the Overhauser nuclear polarization effect, *Phys. Rev.* 102 (1956) 975.
- [3] K.H. Hausser, D. Stehlik, Dynamic nuclear polarization in liquids, *Advances in Magnetic and Optical Resonance*, Elsevier1968, pp. 79-139.
- [4] J.H. Ardenkjaer-Larsen, I. Laursen, I. Leunbach, G. Ehnholm, L.G. Wistrand, J. S. Petersson, K. Golman, EPR and DNP properties of certain novel single electron contrast agents intended for oximetric imaging, *J. Magn. Reson.* 133 (1998) 1-12.
- [5] R.A. Wind, J.H. Ardenkjaer-Larsen, 1H DNP at 1.4 T of water doped with a triarylmethyl-based radical, *J. Magn. Reson.* 141 (1999) 347-354.
- [6] M. Levien, M. Hiller, I. Tkach, M. Bennati, T. Orlando, Nitroxide derivatives for dynamic nuclear polarization in liquids: The role of rotational diffusion, *J. Phys. Chem. Lett.* 11 (2020) 1629-1635.
- [7] M. Levien, M. Reinhard, M. Hiller, I. Tkach, M. Bennati, T. Orlando, Spin density localization and accessibility of organic radicals affect liquid-state DNP efficiency, *PCCP* 23 (2021) 4480-4485.
- [8] D. Yoon, A.I. Dimitriadis, M. Soundararajan, C. Caspers, J. Genoud, S. Alberti, E. de Rijk, J.P. Ansermet, High-field liquid-state dynamic nuclear polarization in microliter samples, *Anal. Chem.* 90 (2018) 5620-5626.
- [9] T. Dubroca, A.N. Smith, K.J. Pike, S. Froud, R. Wylde, B. Trociewicz, J. Mckay, F. Mentink-Vigier, J. van Tol, S. Wi, W. Brey, J.R. Long, L. Frydman, S. Hill, A quasi-optical and corrugated waveguide microwave transmission system for simultaneous dynamic nuclear polarization NMR on two separate 14.1 T spectrometers, *J. Magn. Reson.* 289 (2018) 35-44.
- [10] W. Mullerwarmuth, K. Meisegresch, Molecular motions and interactions as studied by dynamic nuclear-polarization (Dnp) in free-radical solutions, *Adv. Magn. Reson.* 11 (1983) 1-45.
- [11] N.M. Loening, M. Rosay, V. Weis, R.G. Griffin, Solution-state dynamic nuclear polarization at high magnetic field, *J. Am. Chem. Soc.* 124 (2002) 8808-8809.
- [12] C. Griesinger, M. Bennati, H.M. Vieth, C. Luchinat, G. Parigi, P. Hofer, F. Engelke, S.J. Glaser, V. Denysenkov, T.F. Prisner, Dynamic nuclear polarization at high magnetic fields in liquids, *Prog. Nucl. Mag. Res. Sp.* 64 (2012) 4-28.
- [13] T. Orlando, R. Dervisoglu, M. Levien, I. Tkach, T.F. Prisner, L.B. Andreas, V. P. Denysenkov, M. Bennati, Dynamic nuclear polarization of (13) C Nuclei in the liquid state over a 10 tesla field range, *Angew. Chem. Int. Ed. Engl.* 58 (2019) 1402-1406.
- [14] T. Orlando, I. Kuprov, M. Hiller, Theoretical analysis of scalar relaxation in 13C-DNP in liquids, *J. Magn. Reson. Open* 10-11 (2022), 100040.
- [15] P. Hofer, G. Parigi, C. Luchinat, P. Carl, G. Guthausen, M. Reese, T. Carlomagno, C. Griesinger, M. Bennati, Field dependent dynamic nuclear polarization with radicals in aqueous solution, *J. Am. Chem. Soc.* 130 (2008) 3254-+.
- [16] G.Q. Liu, M. Levien, N. Karschin, G. Parigi, C. Luchinat, M. Bennati, One-thousand-fold enhancement of high field liquid nuclear magnetic resonance signals at room temperature, *Nat. Chem.* 9 (2017) 676-680.
- [17] G. Parigi, E. Ravera, M. Fragai, C. Luchinat, Unveiling protein dynamics in solution with field-cycling NMR relaxometry, *Prog. Nucl. Mag. Res. Sp.* 124 (2021) 85-98.
- [18] D.H. Dai, X.W. Wang, Y.W. Liu, X.L. Yang, C. Glauwitz, V. Denysenkov, X. He, T. Prisner, J.F. Mao, Room-temperature dynamic nuclear polarization enhanced NMR spectroscopy of small biological molecules in water, *Nat. Commun.* 12 (2021).
- [19] K.H. Hausser, Dynamic nuclear polarisation in liquids at high magnetic fields, *J. Chim. Phys. Phys.- Chim. Biol.* 61 (1964) 204-209.
- [20] M.G. Concilio, I. Kuprov, L. Frydman, J-Driven dynamic nuclear polarization for sensitizing high field solution state NMR, *PCCP* 24 (2022) 2118-2125.
- [21] M. Reese, D. Lennartz, T. Marquardsen, P. Hofer, A. Tavernier, P. Carl, T. Schippmann, M. Bennati, T. Carlomagno, F. Engelke, C. Griesinger, Construction of a liquid-state NMR DNP shuttle spectrometer: First experimental results and evaluation of optimal performance characteristics, *Appl. Magn. Reson.* 34 (2008) 301-311.
- [22] M.G. Concilio, L. Frydman, Microwave-free J-driven dynamic nuclear polarization: A proposal for enhancing the sensitivity of solution-state NMR, *Phys. Rev. E* 107 (2023), 035303.
- [23] A. Redfield, The theory of relaxation processes, *Advances in Magnetic and Optical Resonance*, Elsevier1965, pp. 1-32.
- [24] L. Yong, J. Harbridge, R.W. Quine, G.A. Rinard, S.S. Eaton, G.R. Eaton, C. Mailer, E. Barth, H.J. Halpern, Electron spin relaxation of triarylmethyl radicals in fluid solution, *J. Magn. Reson.* 152 (2001) 156-161.
- [25] R. Owenius, G.R. Eaton, S.S. Eaton, Frequency (250 MHz to 9.2 GHz) and viscosity dependence of electron spin relaxation of triarylmethyl radicals at room temperature, *J. Magn. Reson.* 172 (2005) 168-175.
- [26] H. Sato, S.E. Bottle, J.P. Blinco, A.S. Micallef, G.R. Eaton, S.S. Eaton, Electron spin-lattice relaxation of nitroxyl radicals in temperature ranges that span glassy solutions to low-viscosity liquids, *J. Magn. Reson.* 191 (2008) 66-77.
- [27] V. Meyer, S.S. Eaton, G.R. Eaton, X-band electron spin relaxation times for four aromatic radicals in fluid solution and comparison with other organic radicals, *Appl. Magn. Reson.* 45 (2014) 993-1007.
- [28] A.A. Kuzhelev, D.V. Trukhin, O.A. Krumkacheva, R.K. Strizhakov, O. Y. Rogozhnikova, T.I. Troitskaya, M.V. Fedin, V.M. Tormyshev, E.G. Bagryanskaya, Room-temperature electron spin relaxation of triarylmethyl radicals at the X- and Q-bands, *J. Phys. Chem. B* 119 (2015) 13630-13640.
- [29] H. Hogben, M. Krzystyniak, G. Charnock, P. Hore, I. Kuprov, Spinach - a software library for simulation of spin dynamics in large spin systems, *J. Magn. Reson.* 208 (2011) 179-194.
- [30] M.G. Concilio, M. Soundararajan, L. Frydman, I. Kuprov, High-field solution state DNP using cross-correlations, *J. Magn. Reson.* 326 (2021).
- [31] I. Kuprov, N. Wagner-Rundell, P. Hore, Bloch-Redfield-Wangsness theory engine implementation using symbolic processing software, *J. Magn. Reson.* 184 (2007) 196-206.
- [32] I. Kuprov, D.M. Hodgson, J. Kloesges, C.I. Pearson, B. Odell, T.D. Claridge, Anomalous nuclear overhauser effects in carbon-substituted aziridines: scalar cross-relaxation of the first kind, *Angew. Chem. Int. Ed.* 54 (2015) 3697-3701.
- [33] L. Lumata, Z. Kovacs, A.D. Sherry, C. Malloy, S. Hill, J. van Tol, L. Yu, L. Song, M. E. Merritt, Electron spin resonance studies of trityl OX063 at a concentration optimal for DNP, *PCCP* 15 (2013) 9800-9807.
- [34] J.J. Jassoy, A. Meyer, S. Spicher, C. Wuebben, O. Schiemann, Synthesis of nanometer sized bis- and tris-trityl model compounds with different extent of spin-spin coupling, *Molecules* 23 (2018).
- [35] D. Margraf, B.E. Bode, A. Marko, O. Schiemann, T.F. Prisner, Conformational flexibility of nitroxide biradicals determined by X-band PELDOR experiments, *Mol. Phys.* 105 (2007) 2153-2160.
- [36] N. Fleck, T. Hett, J. Brode, A. Meyer, S. Richert, O. Schiemann, C-C cross-coupling reactions of trityl radicals: Spin density delocalization, exchange coupling, and a spin label, *J. Org. Chem.* 84 (2019) 3293-3303.
- [37] G.I. Likhtenstein, Nitroxides Brief History, Fundamentals, and Recent Developments Springer Nature, Switzerland2020.
- [38] V.P. Denysenkov, M.J. Prandolini, A. Krahn, M. Gafurov, B. Endeward, T.F. Prisner, High-field DNP spectrometer for liquids, *Appl. Magn. Reson.* 34 (2008) 289-299.
- [39] S. Schott, E.R. McNellis, C.B. Nielsen, H.Y. Chen, S. Watanabe, H. Tanaka, I. McCulloch, K. Takimiya, J. Sinova, H. Sirringhaus, Tuning the effective spin-orbit coupling in molecular semiconductors, *Nat. Commun.* 8 (2017).
- [40] R. Sharp, Closed-form expressions for level-averaged electron spin relaxation times outside the Zeeman limit: application to paramagnetic NMR relaxation, *J. Magn. Reson.* 154 (2002) 269-279.
- [41] R.R. Ernst, G. Bodenhausen, A. Wokaun, Principles of nuclear magnetic resonance in one and two dimensions, Clarendon Press, Oxford, 1987.
- [42] S. Vega, Fictitious spin 1-2 operator formalism for multiple quantum Nmr, *J. Chem. Phys.* 68 (1978) 5518-5527.
- [43] J. Blicharski, Nuclear magnetic relaxation by anisotropy of the chemical shift, *Z. Naturforsch. Pt. A* 27 (1972) 1456.
- [44] I. Tkach, I. Bejenke, F. Hecker, A. Kehl, M. Kasanmaschegg, I. Gromov, I. Prisecaru, P. Hofer, M. Hiller, M. Bennati, H-1 high field electron-nuclear double resonance spectroscopy at 263 GHz/9.4 T, *J. Magn. Reson.* 303 (2019) 17-27.